Applied Catalysis B: Environmental 125 (2012) 197–205

Contents lists available at SciVerse ScienceDirect

Applied Catalysis B: Environmental

journal homepage: www.elsevier.com/locate/apcatb

Using pyridine as nitrogen-rich precursor to synthesize Co-N-S/C non-noble metal electrocatalysts for oxygen reduction reaction

Jinli Qiao[a,*], Li Xu[a], Lei Ding[a], Lei Zhang[b], Ryan Baker[b], Xianfeng Dai[a], Jiujun Zhang[b,*]

[a] College of Environmental Science and Engineering, Donghua University, 2999 Ren'min North Road, Shanghai 201620, PR China
[b] National Research Council Canada, 4250 Wesbrook Mall Vancouver, BC, V6T 1W5, Canada

ARTICLE INFO

Article history:
Received 14 February 2012
Received in revised form 5 May 2012
Accepted 31 May 2012
Available online 7 June 2012

Keywords:
Non-noble metal catalysts
Cobalt
Pyridine
Oxygen reduction reaction
Fuel cells
Metal–air batteries

ABSTRACT

The development of non-noble metal catalysts is of great interest due to their significant potential application in both fuel cell systems and metal–air batteries, particularly when considering long term commercial deployment. In this regard, novel Co-N-S/C non-noble metal catalysts supported on carbon, are synthesized in this study using a solvent-milling method followed by heat-treatment at elevated temperatures. Pyridine is used as the nitrogen-rich ligand for Co-N_x precursor complex formation. The morphology and composition of the catalyst are characterized by X-ray diffraction (XRD), energy-dispersive X-ray (EDX) spectroscopy, transmission electron microscopy (TEM) as well as X-ray photoelectron spectroscopy (XPS). Several catalysts containing different amounts of Co are also synthesized. The optimal Co content is found to be in the range of 10–15 wt% nominal, in terms of catalytic oxygen reduction reaction (ORR) activity. This catalyst shows high electroactivity for the ORR with a high stability in alkaline media. Using rotating disk electrode measurements, and Koutechy–Levich analysis, the overall electron transfer number in the catalyzed ORR is found to be 3.8–4.0, suggesting the catalyzed ORR is a four-electron transfer process from O_2 to H_2O.

1. Introduction

The cathodic oxygen reduction reaction (ORR) is the most challenging step and hence dominates the overall devices' performance for two promising electrochemical energy conversion technologies: polymer electrolyte membrane fuel cells; and metal–air batteries [1,2]. Although Pt-based electrocatalysts, which are used to catalyze the ORR, have been traditionally employed as both the most promising and active catalysts, their high cost has limited both devices' technical maturity and commercialization [3]. To overcome this challenge, two approaches are being actively pursued: the first is to reduce Pt loading, and the second is to explore non-noble catalysts. It seems that non-noble metal catalysts are the best option in terms of a long-term and sustainable solution [4].

Among the different types of non-noble metal catalysts, including non-pyrolyzed and pyrolyzed transition metal nitrogen-containing complexes, conductive polymer-based catalysts, transition metal chalcogenides, metal oxides/carbides/nitrides/oxynitrides/carbonitrides, and enzymatic compounds [5], pyrolyzed transition metal nitrogen-containing complexes supported on carbonaceous materials (M-N_x/C, M = Fe and/or Co) are considered the most promising ORR catalysts because they have demonstrated ORR activity and stability close to that of commercially available Pt/C catalysts [6–9]. However, compared to Pt-based catalysts for practical application in fuel cells, or metal–air batteries, both the ORR activity and stability of these M-N_x/C catalysts have to be significantly improved. In the effort to improve catalytic activity and stability, both the nitrogen-containing ligand, which is used to form a Fe- or Co-complex for the precursor, and its chemical structure, have been identified to play a considerable role [10,11]. However, these nitrogen-containing ligands have complex structures and come at a high cost. Therefore, using more common and cost-effective ligands may be more practical.

In this paper, we employed common and cost-effective pyridine as the nitrogen-rich ligand to form the Co-pyridine complex precursor through a solid-state reaction, which was then pyrolyzed to form a carbon supported ORR catalyst. The catalyst activity was then tested in alkaline solutions using both cyclic voltammetry and rotating disk electrode techniques, since the use of alkaline media presents many advantages over acidic solution due to the less corrosive environment and faster kinetics for oxygen reduction. Several sophisticated instrument methods such as crystal-phase X-ray diffraction (XRD), transmission electron microscopy (TEM), energy dispersive X-ray (EDX) spectroscopy and X-ray photoelectron spectroscopy (XPS) were used for catalyst morphology analysis.

* Corresponding authors. Tel.: +86 21 67792379; fax: +86 21 67792159.
E-mail addresses: qiaojl@dhu.edu.cn, qiaojinli@hotmail.com (J. Qiao), jiujun.zhang@nrc.gc.ca (J. Zhang).

0926-3373/$ – see front matter © 2012 Elsevier B.V. All rights reserved.
http://dx.doi.org/10.1016/j.apcatb.2012.05.050

2. Experimental

2.1. Catalyst synthesis

For catalyst preparation, cobalt sulfate heptahydrate ($CoSO_4{\cdot}7H_2O$) and pyridine, both "analytically pure" grade were purchased from Guoyao, Shanghai. They were first mixed, and the formed mixture was then mixed with a corresponding amount of Vulcan carbon (Vulcan XC-72R with a BET of 235 $m^2\,g^{-1}$, purchased from Cabot) to form the precursor mixture. In this new mixture, the carbon content was controlled at 60 wt%, and the sum weight percentage of $CoSO_4{\cdot}7H_2O$ plus pyridine was controlled at 40 wt%. The weight percentage ratio of $CoSO_4{\cdot}7H_2O$ to pyridine could be adjusted according to the needs of the experiment. Note that the Co loading with respect to carbon could be adjusted in a range from 2 to 20 wt%. For the solid-state reaction, the formed precursor mixture above was dispersed in 10 mL methanol solvent while milling in a mortar for 2 h, which was then dried in a vacuum at 40 °C for 1 h to form a powder. This powder was further processed by thermal treatment under N_2 atmosphere at temperatures of 200, 400, 600, 800 and 900 °C, respectively, for 2 h to optimize the heat-treatment temperature with respect to the ORR electrocatalytic activity. The resulting catalyst powders, characterized by crystal-phase XRD described below, contained C, Co and S, therefore, the catalyst was expressed as Co-N-S/C in this paper. To elucidate the effect of cobalt alone, a baseline sample of carbon loaded with metal-free pyridine was also prepared under the same conditions described above, and is expressed as N/C in this paper.

2.2. Catalyst physical characterization

For physical characterization of the samples, crystal-phase XRD patterns were collected on a Rigaku D/max-2550 V diffractometer using Cu Kα radiation (λ = 0.15406 nm) and operating at 30 kV and 40 mA. TEM analyses for the samples were performed on a high-resolution Hitachi JEM-2100 system operating at 200 kV to obtain information about the distribution of carbon and the metal particles. The catalyst bulk composition (C, N, O, S, Co) was verified by means of EDX on JSM-5600LV (JEOL) attached to field emission scanning electron microscope (FE-SEM) on Oxford IE 300 X. Surface analysis of the catalyst particles was carried out by XPS on a RBD upgraded PHI-5000C ESCA system (PerkinElmer) with Al K X-ray anode source ($h\nu$ = 1486.6 eV) at 250 W and 14.0 kV.

2.3. Electrode preparation

For working electrode preparation, a pre-cleaned rotating disk electrode (RDE) (glassy carbon electrode with a disk diameter of 6.0 mm (corresponding to a geometric surface area of 0.28 cm^2), purchased from Pine Instruments) was coated with catalyst to form the catalyst layer. The catalyst ink for this purpose was prepared by ultrasonically mixing 4.0 mg catalyst with 2.0 mL of isopropyl alcohol. 10.0 μL of this ink was then deposited onto the GC surface to form a uniform layer across the electrode surface. After drying, one drop of methanol/Nafion® solution (50:1 wt%) was then deposited onto the top of the catalyst layer to protect the catalyst from falling off during the electrochemical measurements. Note that the proton exchange Nafion® ionomer used here can be converted into the potassium exchange Nafion® ionomer when the coated electrode was measured in KOH solution. The overall catalyst loading of the catalyst was 70.6 $\mu g\,cm^{-2}$.

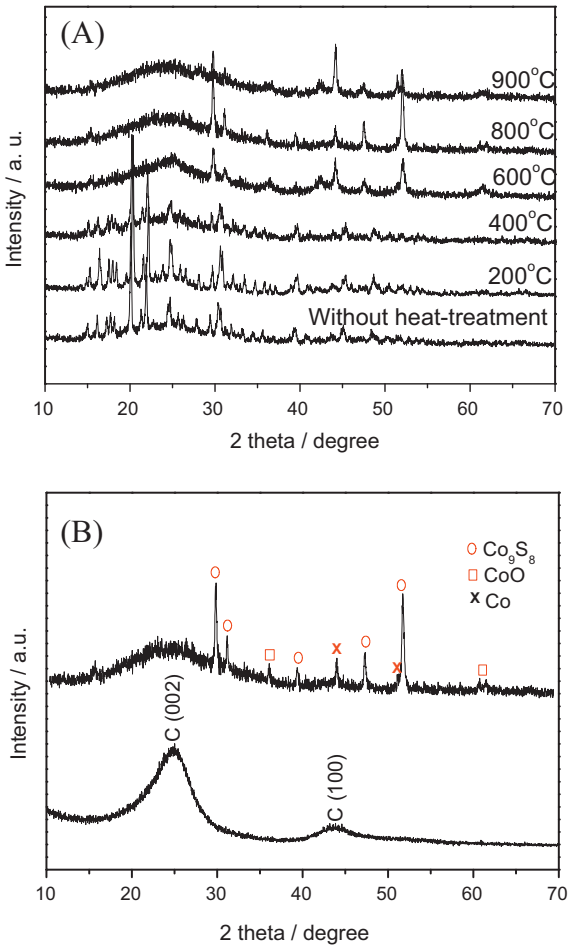

Fig. 1. XRD patterns of (A) the Co-N-S/C catalysts obtained at different heat-treatment temperatures, and (B) Co-N-S/C catalyst obtained at 800 °C as well as Vulcan X-72 with all peak positions marked. The Co-N-S/C catalyst used is $Co_{15\,wt\%}$-$Py_{25\,wt\%}$/C heat-treated for 2 h.

2.4. Electrochemical measurements

For catalyst ORR activity, all electrochemical measurements were performed in a standard three-compartment cell at 25 °C. A Pt wire and a saturated calomel electrode (SCE) were used as the counter, and reference electrodes, respectively. All measured potentials were converted to the standard hydrogen electrode (SHE). For cyclic voltammograms (CVs), the electrode was scanned at a scan rate of 50 $mV\,s^{-1}$ in the potential range between −0.30 and 0.60 V to measure the surface behavior of the catalyst in N_2-saturated KOH solution, and the ORR activity of the catalyst in O_2-saturated KOH solutions, respectively. For more quantitative measurements of ORR activity, linear sweep voltammetry (LSV) was conducted on the catalyst-coated RDE in the potential range between −0.30 and 0.15 V at a scan rate of 5 $mV\,s^{-1}$ in O_2-saturated KOH solution at various rates of rotation. In addition, various concentrations of KOH solutions ranging from 0.1 to 3.0 M were employed to study the effect of KOH concentration on the ORR catalytic activity.

3. Results and discussion

3.1. Physical characterization

Fig. 1(A) shows the XRD patterns of the catalyst synthesized before and after heat treatment at 200, 400, 600, 800 and

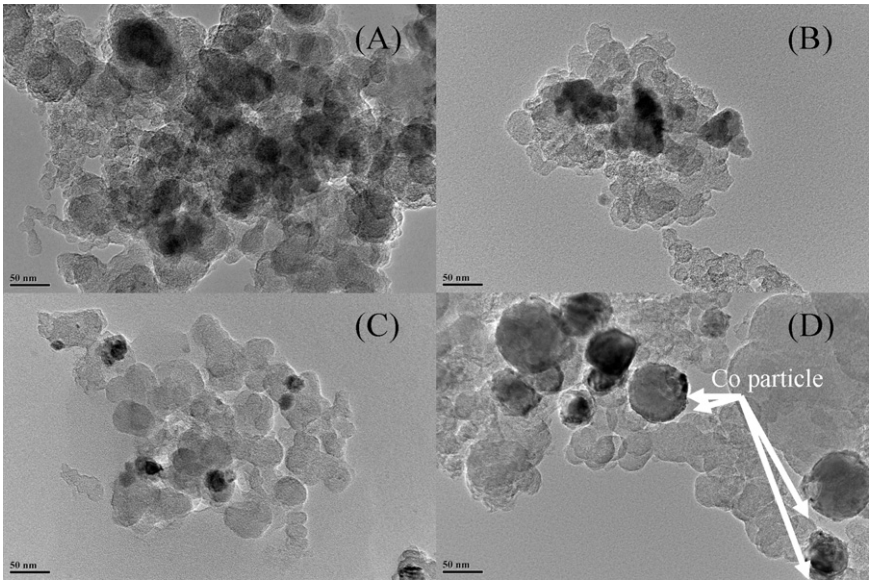

Fig. 2. TEM images of (A) Co^{II}-Py/C without heat-treatment, (B) Co-N-S/C obtained at 600 °C heat-treatment, (C) Co-N-S/C obtained at 800 °C heat-treatment and (D) Co-N-S/C obtained at 900 °C heat-treatment. The Co-N-S/C catalyst used is $Co_{15\,wt\%}$-$Py_{25\,wt\%}$/C heat-treated for 2 h.

900 °C, respectively. Comparing catalysts with and without heat-treatment, several characteristic diffraction peaks appear after heat-treatment. A more detailed view is shown in Fig. 1(B) where all peak positions are marked on the top pattern (catalyst obtained by heat-treatment at 800 °C), while the bottom curve shows the sample of Vulcan X-72. These peaks could be assigned to a mixture of the metallic phases containing β-Co at 44.3° and 51.2° [12,13], CoO and/or Co_9S_8 at 30°, 31.1°, 47° and 52.5° (Fig. 1A), respectively, as well as a broad diffraction peak from carbon black at 24.9° (Fig. 1B). In addition, the magnitude of both crystalline peaks observed at 44.3° and 51.2° (from β-Co) increases with increasing heat-treatment temperature while there is only one weak and broad peak at 44.3° for non-heat treated sample. These results indicate that the structure of the Co^{II}-Py precursor complex may have decomposed into metallic Co, Co oxide, and Co-S compound, during the heat-treatment process. The S in Co_9S_8 should come from SO_4^{2-} anion in $CoSO_4$, while the Co oxide formation could be favored at high temperature through oxygen donation from the $CoSO_4$ anion and/or oxygenated species on the carbon surface. It is also possible that the oxide formation is related to the catalyst exposure to air after being removed from the inert atmosphere.

Fig. 2(A–D) shows typical TEM images for the catalysts synthesized before and after heat treatment at 600, 800 and 900 °C, respectively, to investigate particle size distribution. It can be seen that no clear metal particles appear for non-heat-treated catalyst samples except for some aggregates with an average particle size of 44 nm on the carbon support surface (Fig. 2A). When the catalyst is heat-treated at 600 °C, the aggregate size decreases, and some Co metal particles appear but without a clear shape (Fig. 2B). However, with a further increase in temperature to 800 °C, the existence of metal particles (black dots) with an average particle size of 17 nm are clearly observed, which are uniformly dispersed on the Vulcan XC-72 support (Fig. 2C). With a further increase in temperature up to 900 °C, both small (with an average particle size of 20 nm) and large particles (with an average particle size of 65 nm) can be observed (Fig. 2D). These particles could be attributed to the β-Co phase aggregated on the carbon support surface although the metal particles are encapsulated within the carbon substrates [14–16]. These results suggest that heat-treatment can decompose the Co^{II}-Py complex to metallic Co, which then agglomerates into large particle size when increasing the heat-treatment temperature. This result is in agreement with the observation from the XRD analysis in Fig. 1.

To determine catalyst cobalt content, EDX analysis was employed to analyze both non-heat-treated and heat-treated catalyst samples. As shown in Fig. 3(A), total Co content is measured to be 22.7 wt% for the catalyst synthesized at 800 °C, which is higher than that for the non-heat-treated sample (15 wt%Co in

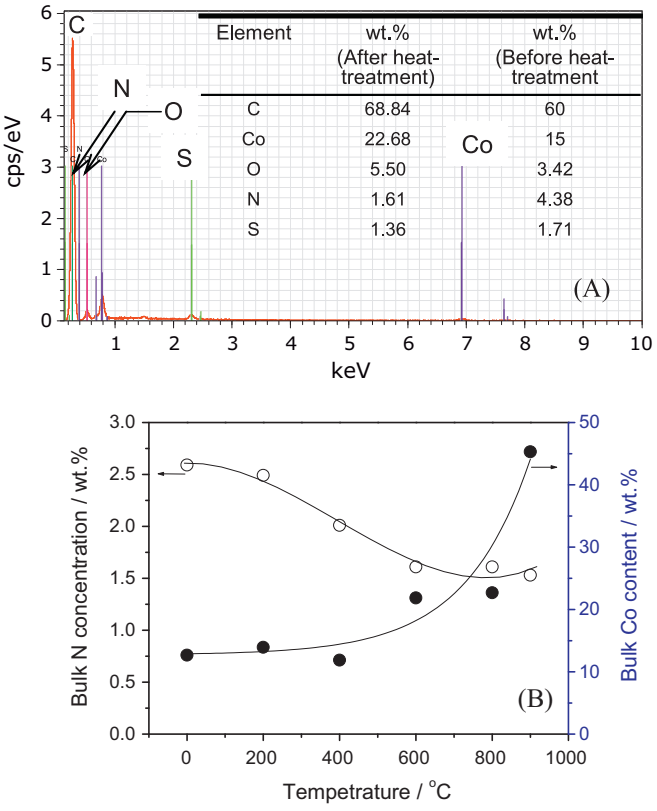

Fig. 3. (A) EDS pattern for Co-N-S/C obtained at 800 °C heat-treatment, (B) bulk N and Co concentration changing with the heat-treatment temperatures. The Co-N-S/C catalyst used is $Co_{15\,wt\%}$-$Py_{25\,wt\%}$/C heat-treated for 2 h.

Table 1
Peak areas of possible active species in the catalyst after heat-treatment at different temperatures. The areas were obtained from XRD results.

Temperature (°C)	Co_9S_8	CoO	Co	CoO/Co_9S_8	Co/Co_9S_8
600	698.8	2021.3	424.3	2.89	0.61
800	355.5	330.7	210.0	0.93	0.59
900	415.0	140.3	1317.2	0.33	3.17

The Co-N-S/C catalyst used is $Co_{15\,wt\%}$-$Py_{25\,wt\%}$/C and heat-treated at 800 °C for 2 h.

Co^{II}-Py/C). This indicates that pyridine decomposition happened in the Co^{II}-Py/C complex during heat-treatment. From Fig. 3(A), it can be calculated that the total N content in the heat-treated sample is about 1.6 wt%. If assuming that all of these N atoms are coordinated by Co ions to form ORR active sites (Co-N_4) [17,18], 1.7 wt% of Co will be used. However, the total Co content is 22.7 wt% as measured by EDX, suggesting that other 21 wt% of Co exist in the forms of metallic Co, Co oxides, and Co-S compounds, which may not be ORR active. Fig. 3(B) shows both N and Co content as a function of heat-treatment temperature. It can be seen that the total N content decreases with increasing temperature, while the bulk Co concentration (wt%) increases significantly with temperature. This increase in Co content is mainly due to the decompositions of: carbon (forming CH_4 gas), pyridine, H_2O attached on $CoSO_4$ and/or part SO_4^{2-}. The decrease in N content might be due to pyridine decomposition. It should be mentioned that although N content (indicated in the inserted table in Fig. 3(A)) is high at low temperatures, it is not involved in forming ORR Co-N_x active centers, but only contained in Co-Pyridine complexes. Only when the complex is pyrolyzed, can the Co-N_x active center be formed. Note that, the total content in the right column of the table inserted in Fig. 3(A) is not 100 wt%, instead it is 84.5 wt%. The remaining 15.5 wt% is water content, which is not listed. After heat-treatment, all water was removed from the sample. This is why the total content in the left column of the inserted table in Fig. 3(A) is 100 wt%. The carbon content increased from 60 to 68.8 wt% mainly because of water removal.

The interesting result is that the presence of S can be detected in the catalyst using both XRD and EDX. S was not detected when using the most commonly metal precursor such as $Co(NO_3)_2$ [14,19,20]. In our experiments, using $CoCl_2{\cdot}6H_2O$ as the Co-precursor instead of $Co(SO_4){\cdot}7H_2O$, we found that the ORR onset potential on catalyst synthesized using this Co-precursor is 50 mV lower than that for the Co-N-S/C catalyst synthesized using $CoSO_4$ as the Co-precursor, indicating the presence of S can benefit the ORR activity. For understanding the effect of S in the catalyst further, we measured the content of Co, CoO and S in the catalyst and also the ratio of CoO/Co_9S_8 and Co/Co_9S_8 by XRD using the integral peak area (Table 1). It is interesting to find that peak area of metallic Co in the catalyst heat-treated at 900 °C is more than 6-fold of metallic Co in the catalyst heat-treated at 800 °C. Also, the catalyst heat-treated at 600 °C gives the high peak area of CoO and metallic Co compared to the catalyst heat-treated at 800 °C. In particular, both the ratios of CoO/Co_9S_8 and Co/Co_9S_8 in the catalysts heat-treated at 600 and 900 °C are much larger than that at 800 °C. Therefore, it can be concluded that the porosity of the catalyst is highly blocked by CoO and metallic Co due to the decomposition of Co(II)-pyridine, which are not active for the ORR. That is why we observed a higher ORR activity for the catalyst heat-treated at 800 °C than that of catalysts heat-treated at other temperatures. This is also discussed in further detail below.

In order to detect Co-N_x on the catalyst surface, XPS measurements were used to determine the chemical state of surface catalyst particles. The Co $2p_{3/2}$, N ls, O ls, S 1s and C ls core levels of the catalyst materials were recorded for both the non-heat-treated sample (Co^{II}-Py/C) and the heat-treated sample (Co-N-S/C). The heat-treated sample obtained at 800 °C was selected as the target analysis material. As shown in Fig. 4(A), two bands can be clearly observed, which correspond to lower energy (Co $2p_{3/2}$) and higher energy (Co $2p_{1/2}$) asymmetric bands originating from spin–orbital splitting [21,22]. For the non-heat-treated sample, the Co $2p_{3/2}$ peak has a binding energy of approximately 782.15 eV [22,23], which is attributed to Co in an oxidation state. Metallic Co has a binding energy of 777.9 eV, while CoO and Co_2O_3 have binding energies of 780 eV and 779.4 eV, respectively [23]. After heat-treatment, some slightly positive shifts in both Co $2p_{1/2}$ and Co $2p_{3/2}$ binding energy positions are observed (796.95 eV and 780.62 eV), indicating that Co obtains a higher oxidation state. Because the oxidation state of Co in the non-heat-treated catalyst is Co(II), it is believed that after heat-treatment, part of the Co(II) is converted into Co(III). As yet, compared to non-heat-treated sample, after the heat treatment, the shift in Co $2p_{3/2}$ peak to lower binding energy indicates that Co becomes more reduced during this process. The loss of Co signal after heat-treatment indicates that the Co becomes encapsulated with carbon upon heating, which is consistent with TEM analysis as observed in Fig. 2

Table 2
Concentrations (at%) of C, N, O, S and Co in the Co-N-S/C catalyst obtained before and after the heat-treatment at 800 °C, determined by XPS.

	C	N	O	S	Co
Before heat treatment	87.75	0.96	7.96	1.26	1.89
After heat treatment	93.86	0.29	3.60	0.89	1.36

The Co-N-S/C catalyst used is $Co_{15\,wt\%}$-$Py_{25\,wt\%}$/C.

Fig. 4(B) shows the N 1s binding energy region, where the peaks of N 1s at 399.9 and 401.3 eV can be attributed to pyridinic-N-H and graphitic-N, respectively [11,14–16,24]. In this work, the N 1s peaks at 398.3 are attributed to pyridinic-N for non-heat-treated sample which was not the same as reported elsewhere, where instead ethylenediamine (EDA) [15,16], 2,3,5,6-tetra(2-pyridyl)pyrazine [11], and phthalocyanine [25], were used as the N-precursors. The high-temperature pyrolysis induced significant nitrogen loss from 0.96 to 0.29 at% (Table 2). In this case, the signal is not clear due to the large amount of noise, however, we could still identify a very weak XPS peak of N 1s. The deconvolution of the N signals after heat-treatment at 800 °C gives three bands with binding energies of 398.3, 401.1 and 404.8 eV, respectively, which could be assigned to pyridinic-N, graphitic-N (quaternary-N) and pyridine-N-oxide, respectively. Both pyridinic-N and graphitic-N are believed to be those coordinated by Co ions on the surface, forming ORR active sites [11,14–16,24]. It is noted that the pyrrolic-N/pyridone-N peak in the N 1s spectra of non-heat-treated sample (Co^{II}-Py/C) disappeared in the N 1s spectra of the heat-treated sample (Co-N-S/C) at 800 °C, accompanied by an increased peak intensity for graphitic-N. Niwa et al. [24] also found the same results for pyrolyzed CoPc/C using X-ray absorption analysis, where the catalysts with a relatively larger amount of graphite-like nitrogen exhibited a higher ORR activity than those with a relatively larger amount of pyridine-like nitrogen. On the other hand, carbon alloys synthesized by the pyrolysis of nitrogen-containing precursors contained a large amount of graphite-like nitrogen. As observed, the non-heat-treated sample (with some graphitic-N) could be also active for the ORR, therefore, it seems reasonable to assert that both

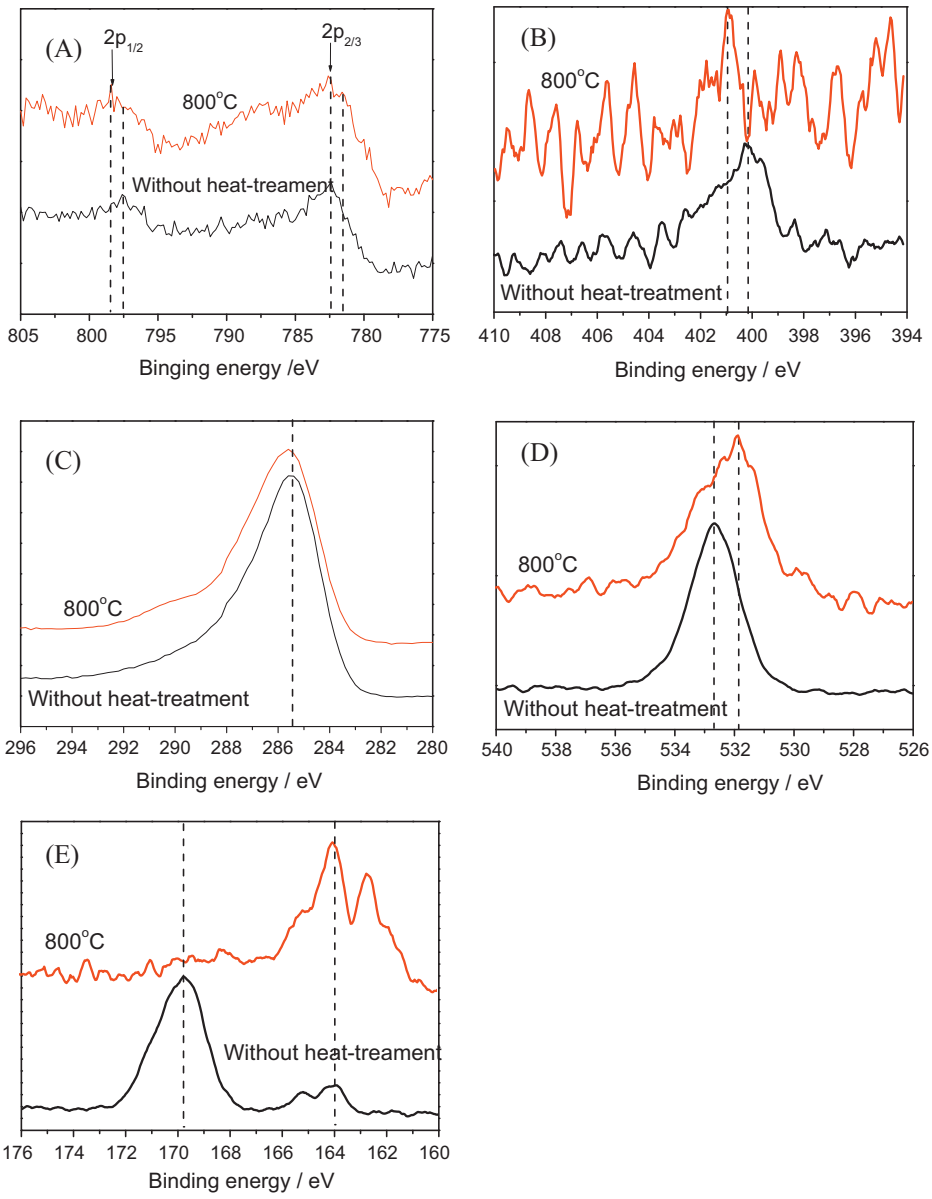

Fig. 4. XPS spectra of (A) Co 2p, (B) N 1s, (C) C 1s, (D) O 1s and (E) S 2p for the Co-N-S/C catalyst before and after the heat-treatment at 800 °C. The Co-N-S/C catalyst used is $Co_{15\,wt\%}$-$Py_{25\,wt\%}$/C heat-treated for 2 h.

graphitic-N and pyridinic-N bonded by Co ion in this work should be mainly responsible for the increased number of oxygen reduction active sites which facilitates oxygen adsorption.

From Fig. 4(C), the peaks of C 1s at 285.4 ± 0.2 eV can be clearly observed. These peaks are attributed to C sp^3 that could be assigned to the amorphous carbon substrate, or the C—N single bonds formed during the heat treatment process [11]. Compared to the non-heat-treated catalyst sample, no obvious change is observed for the heat-treated catalyst sample for the C 1s band position at 285.4 ± 0.2 eV. It can be concluded, therefore, that the main contribution to this band should come from the C sp^3 bonds in the carbon substrate. However, the C 1s signals become much broader for the heat-treated samples, which suggests that some additional C—N single bonds are formed during heat-treatment. The small shoulders at 289.5–290.7 eV are usually assigned to carbon in the form of C═O and C—O, respectively. The results obtained for the O 1s spectral region are presented in Fig. 4(D). The band at 533.5 ± 0.1 eV may be related to C—O in carboxylic, epoxy, or phenol groups on the carbon substrate. It has been suggested that catalysts prepared under severe pyrolysis conditions are sensitive to oxidation in ambient air – even at room temperature. The shift of O 1s peak to lower binding energies for heat-treated Co-N-S/C compared to the sample without heat-treatment (Co^{II}-Py/C) could be observed. Therefore, XPS spectra from carbon are also indicative of the formation of surface O-containing groups, which may help the catalyst activity enhancement together with N and C.

Fig. 4(E) shows S 2p spectra measured for catalyst samples before and after heat-treatment at 800 °C. It can be seen that the catalyst without heat-treatment shows a large band at 167.0–172.0 eV, which could be assigned to sulfate in catalyst precursor [26]. After heat-treatment, this band disappears almost completely, and transfers to a spectral region at 162.0–167.0 eV as seen in Fig. 5, indicating that some sulfided cobalt may be formed [27]. This is in accordance with XRD results obtained. It was reported that pyrolysis of the catalyst in the presence of sulfur could lead to mainly amorphous carbon, resulting in an increased catalyst porosity and in turn enhanced catalyst performance [28–30]. It is believed that in the absence of sulfur, the decomposition of catalyst precursor

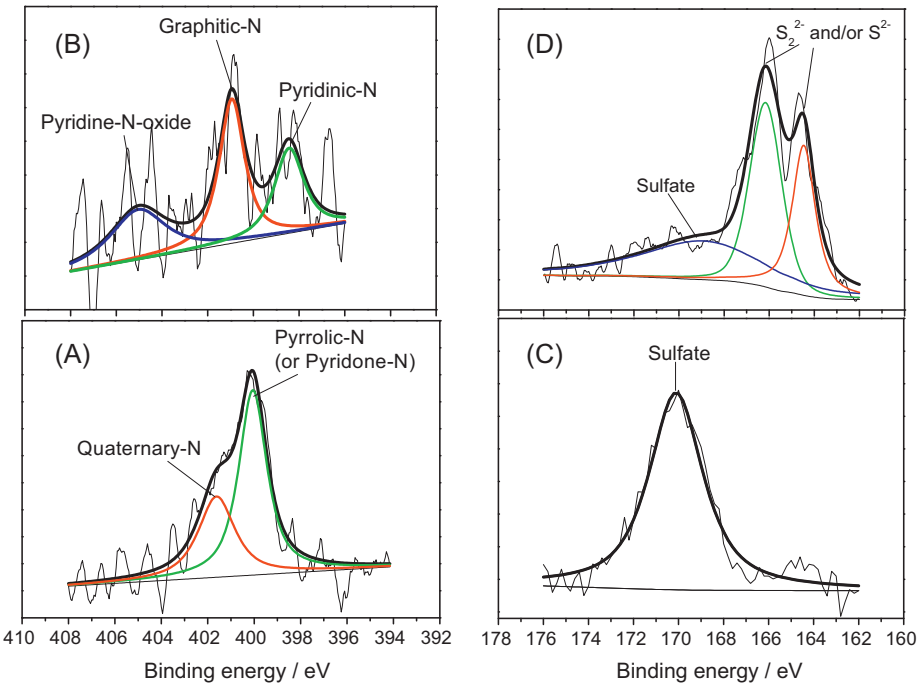

Fig. 5. XPS spectra of deconvoluted N 1s and S 2p for Co-N-S/C catalyst. (A, C) Before heat-treatment; (B, D) after the heat-treatment at 800 °C. The catalyst used is $Co_{15\,wt\%}$-$Py_{25\,wt\%}$/C heat-treated for 2 h. Thin lines are measured data and the bold lines are fitted curves.

could easily form metal carbides during the heat-treatment process. These metal carbides are not active toward the ORR. However, in the presence of sulfur related species, they may be able to reduce the chance forming metal carbide [28–30], resulting in more formation of ORR active centers. Our experiments showed that in the presence of SO_4^{2-}, there was no cobalt carbide that could be detected in the heat-treated catalyst samples, suggesting the sulfur might play such a role in inhibiting the formation of cobalt carbide. Similar to nitrogen in the catalyst, the high-temperature pyrolysis could also induce a significant sulfur loss from 1.26 to 0.98 at% (Table 2). This is probably because the decomposition of Co(II)-pyridine and Co(II)-S complexes to partially form metal Co and some small molecules of N- and S-containing compounds which are blown out along with the inert gas stream. However, it is interesting to note that the content of S is almost 3-fold of N, further indicating that both N and S play the role in improving the ORR activity. As mentioned above, the ORR onset potential on Co-N-S/C catalyst synthesized using $CoSO_4$ as the Co-precursor is 50 mV more positive than that synthesized using $CoCl_2{\cdot}6H_2O$ as the Co-precursor and, suggesting that the presence of sulfur can indeed benefit ORR activity.

3.2. Electrochemical characterization

For electrochemical characterization, Fig. 6(A) shows CVs of the Co-N-S/C catalysts synthesized from a precursor containing 15 wt% of Co, 25 wt% of Py and 60 wt% of carbon heat treated at different temperatures. This precursor is expressed as $Co_{15\,wt\%}$-$Py_{25\,wt\%}$/C. The measurement was carried out in O_2-saturated 3.0 M KOH solution. It can be seen that there are two pairs of redox peaks at −0.30–0.05 V and 0.10–0.35 V vs. SHE, respectively, in particular for the catalyst obtained at 800 °C heat-treatment. With increasing heat-treatment temperature, the magnitudes of these two redox peaks keep increasing until 800 °C. After 800 °C, they decrease, suggesting that ~800 °C may be the optimal temperature in obtaining the most electroactive catalyst. Below 800 °C, with increasing heat-treatment temperature, more Co-N_x active sites could be produced. However, when temperature is higher than 800 °C such as 900 °C, the undesired formation of secondary species can be produced, mainly Co, Co oxide, and Co-S compound as shown in Figs. 1 and 3, which could lead to a reduced concentration of Co-N_x moieties on the catalyst surface. The redox wave at 0.10–0.35 V is believed to be the process of Co^{II}-N-S ↔ Co^{III}-N-S + e^-, and the wave at −0.30–0.05 V to be the process of Co^{I}-N-S ↔ Co^{II}-N-S + e^-. Here the redox couple of Co^{II}-N-S/Co^{III}-N-S should be responsible for ORR activity. Fig. 6(B) shows the ORR curves for the same catalyst in O_2-saturated 3.0 M KOH solution. It can be seen that the ORR onset potentials are fairly close to those for the Co^{II}-N-S/Co^{III}-N-S wave in Fig. 6(A), further suggesting the Co^{II}-N-S/Co^{III}-N-S redox couple should be responsible for ORR activity. Again, the catalyst obtained by heat-treatment at 800 °C gives the best ORR activity. The effect of Co content in the catalyst was also tested using different samples containing different amounts of Co, such as $Co_{2\,wt\%}$-$Py_{38\,wt\%}$/C, $Co_{5\,wt\%}$-$Py_{35\,wt\%}$/C, $Co_{10\,wt\%}$-$Py_{30\,wt\%}$/C, $Co_{15\,wt\%}$-$Py_{25\,wt\%}$/C, and $Co_{20\,wt\%}$-$Py_{20\,wt\%}$/C, respectively. The optimum Co loading was found to be in the range of 10–15 wt%, for which the best ORR activity was observed (Fig. 6(C)). For comparison, several other catalysts, such as commercially available Pt/C, $Co_{40\,wt\%}$/C, and $Py_{40\,wt\%}$/C, were also tested for ORR activity, and the results obtained are shown in Fig. 6(D) together with those for $Co_{10\,wt\%}$-$Py_{30\,wt\%}$/C. Note that for both $Co_{40\,wt\%}$/C and $Py_{40\,wt\%}$/C samples, the heat-treatment temperatures were all at 800 °C, the same as that for $Co_{10\,wt\%}$-$Py_{30\,wt\%}$/C. It can be seen that $Co_{10\,wt\%}$-$Py_{30\,wt\%}$/C has a much higher ORR activity than both those of $Co_{40\,wt\%}$/C and $Py_{40\,wt\%}$/C. However, it is still lower than that for the commercial Pt-based catalyst.

For a more quantitative evaluation of the ORR catalytic activity of the catalysts developed in this work, RDE voltammetry measurements were also carried out at different electrode rotation rates, as shown in Fig. 7(A, B and C), measured in O_2-saturated solution containing three different KOH concentrations such as 0.1, 1.0 and 3.0 M, respectively. Using Koutechy–Levich theory, the overall

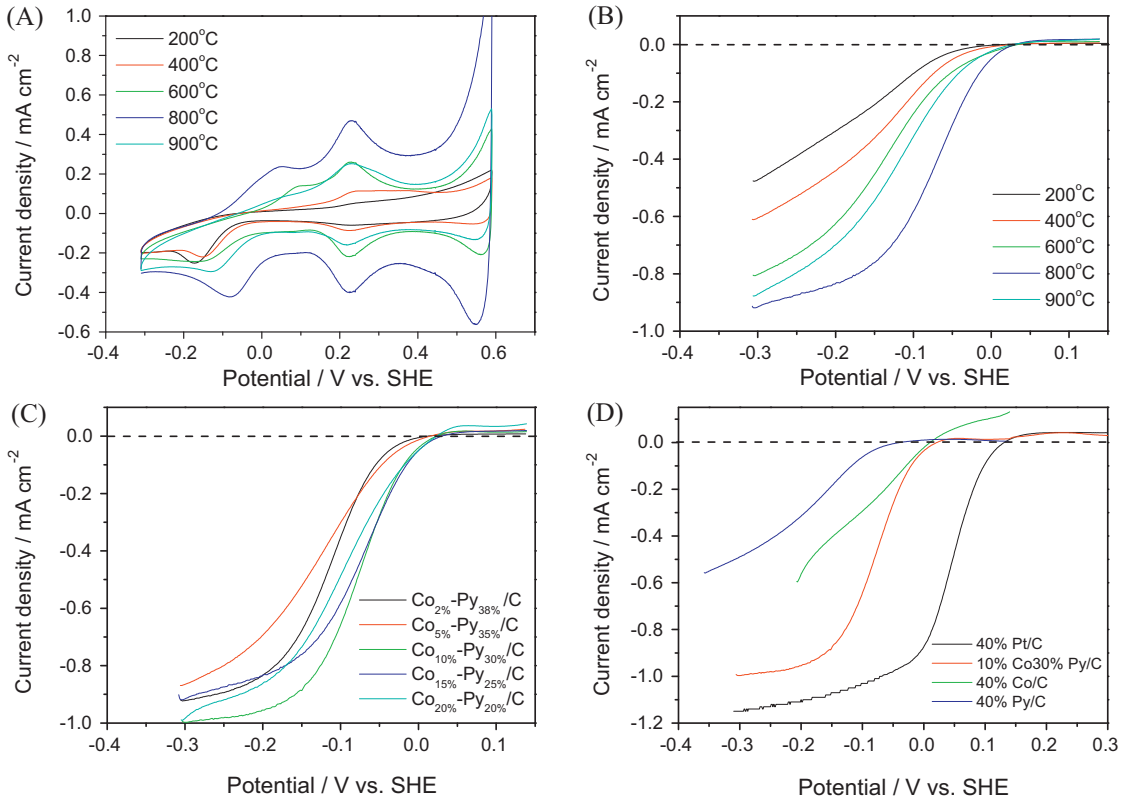

Fig. 6. (A) Cyclic voltammograms of Co-N-S/C catalysts obtained at different heat-treatment temperatures, measured in O_2-saturated 3.0 M KOH solution with a potential scan rate of 50 mV s^{-1}, (B) linear sweep ORR voltammetric curves for Co-N-S/C catalysts obtained at different heat-treatment temperatures, measured in O_2-saturated 3.0 M KOH solution at a scan rate of 5 mV s^{-1}. (C) Linear sweep ORR voltammetric curves for Co-N-S/C catalysts obtained at different Co contents in the catalyst, measured in O_2-saturated 3.0 M KOH solution at a scan rate of 5 mV s^{-1}. The Co-N-S/C catalyst used is $Co_{15\,wt\%}$-$Py_{25\,wt\%}$/C heat-treated at 800 °C for 2 h. (D) Linear sweep voltammetric curves of ORR on different catalysts as marked in the figure, measured in O_2-saturated 3.0 M KOH solution at a scan rate of 5 mV s^{-1}. The Co-N-S/C catalyst used is $Co_{10\,wt\%}$-$Py_{30\,wt\%}$/C heat-treated at 800 °C for 2 h. The electrode rotation rate: 1500 rpm and the catalyst loading: 70.6 μg cm^{-2}.

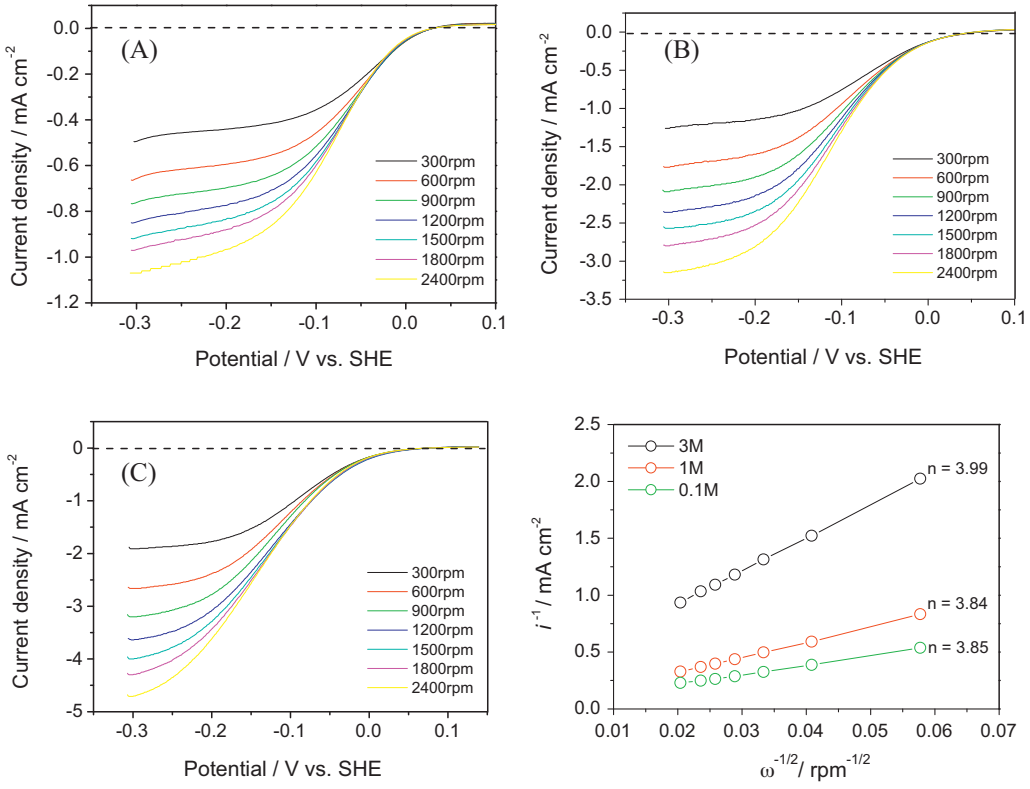

Fig. 7. Linear sweep voltammetric curves of ORR on Co-N-S/C catalyst at various rotation rates in (A) 3.0 M KOH, (B) 1.0 M KOH and (C) 0.1 M KOH. (D) Koutecky–Levich plots for three KOH concentrations at −0.25 V. Potential scan rate: 5 mV s^{-1} and the catalyst loading: 70.6 μg cm^{-2}. The Co-N-S/C catalyst used is $Co_{15\,wt\%}$-$Py_{25\,wt\%}$/C heat-treated at 800 °C for 2 h.

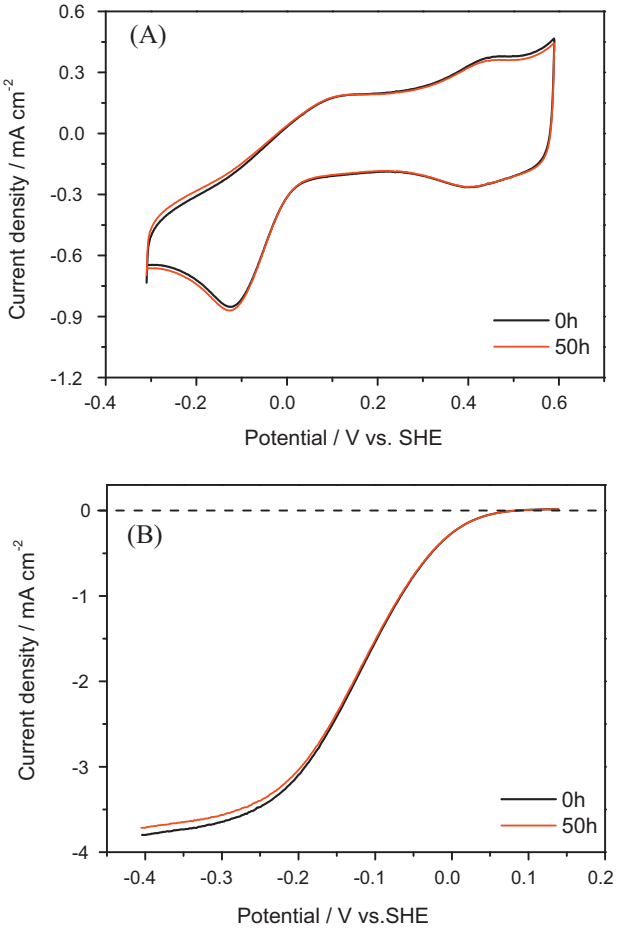

Fig. 8. (A) Cyclic voltammograms, (B) polarization curves for the oxygen reduction reaction on Co-N-S/C in O_2-saturated 0.1 M KOH before and after the potential chronoamperometric test at −0.11 V in O_2-saturated 0.1 M KOH for 50 h. Potential scan rate is 50 mV s^{-1} for cyclic voltammogram and, 5 mV s^{-1} for linear sweep voltammetric curves with electrode rotation rate of 1500 rpm. The catalyst loading: 70.6 μg cm^{-2}. The Co-N-S/C catalyst used is $Co_{10\,wt\%}$-$Py_{30\,wt\%}$/C heat-treated at 800 °C for 2 h.

electron transfer number in the catalyzed ORR can be estimated [31,32]:

$$\frac{1}{i} = \frac{1}{i_k} + \frac{1}{0.2nFC_{O_2}D_{O_2}^{2/3}\nu^{-1/6}}\omega^{-1/2} \quad (1)$$

where i is the disk ORR current density, i_k is the kinetic current density, n is the overall number of electrons transferred per molecule of O_2 reduced, F is Faraday's constant (F = 96485 C mol^{-1}), C_{O_2} is the concentration of oxygen dissolved [33], D_{O_2} is the diffusion coefficient of O_2 in the bulk solution, and ν is the kinetic viscosity of the solution. The constant 0.2 is adopted when the rotation speed is expressed in rpm. By plotting $1/i$ vs. $\omega^{-1/2}$ according to Eq. (1), both the overall electron number (n) and the kinetic current density (i_k) can be estimated. Fig. 7(D) shows the linear relationships between $1/i$ and $\omega^{-1/2}$ at −0.3 V and three KOH concentrations, suggesting that Eq. (1) is valid in this case. From the slopes of these three lines, the overall electron number can be obtained, which are 3.85, 3.84 and 3.99, respectively. These values are fairly close to 4.0, suggesting that the ORR catalyzed by Co-N-S/C catalyst is a four-electron transfer process from O_2 to H_2O at all three KOH solution concentrations.

Regarding the ORR mechanism catalyzed by Co-N-S/C catalyst, and considering a four-electron transfer process, we believe it should go through an inner-sphere mechanism as follows:

$$Co^{III}\text{-N-S/C} + e^- \leftrightarrow Co^{II}\text{-N-S/C} \quad (2)$$

$$Co^{II}\text{-N-S/C} + O_2 \leftrightarrow O_2\text{-}Co^{II}\text{-N-S/C} \quad (3)$$

$$O_2\text{-}Co^{II}\text{-N-S/C} + 4e^- + 2H_2O \rightarrow 4OH^- + Co^{II}\text{-N-S/C} \quad (4)$$

$$Co^{II}\text{-N-S/C} \leftrightarrow Co^{III}\text{-N-S/C} + e^- \quad (5)$$

In this mechanism, the promotion role of the sulfur on the catalyst surface is not clear at this moment. Furthermore, this mechanism is just a proposal to facilitate understanding. More experimental and theoretical approaches are definitely needed to validate it.

3.3. Catalyst stability

For catalyst stability, Fig. 8 shows cyclic voltammograms (Fig. 8(A)) and the polarization curves (Fig. 8(B)) for the oxygen reduction reaction on the Co-N-S/C before and after the potential-chronoamperometric test in 0.1 M KOH, respectively. The potential-chronoamperometric test was carried out at −0.11 V in O_2-saturated 0.1 M KOH for 50 h. The cyclic voltammograms were measured between −0.3 and 0.6 V in O_2-saturated 0.1 M KOH with a scan rate of 50 mV s^{-1}. The polarization curves were measured in O_2-saturated 0.1 M KOH using a scan rate of 5 mV s^{-1} and an electrode rotation rate of 1500 rpm. It can be seen that the experiments running for 50 h show an insignificant decay in current density on the Co-N-S/C ($Co_{15\,wt\%}$-$Py_{25\,wt\%}$/C) electrodes, indicating that the catalyst is stable in alkaline solution under these conditions.

4. Conclusions

A novel non-noble metal catalyst supported on carbon, Co-N-S/C, was synthesized using a solvent-milling method followed by heat-treatment at elevated temperatures. The morphology and composition of the catalyst were characterized by XRD, TEM, EDX as well as XPS. It was found that during the heat-treatment process, the precursor (Co^{II}-Py/C) was decomposed into metallic Co, Co oxide, Co-S compound, graphitic-N, pyridinic-N as well as pyridine-N-oxide. Only a small portion of Co^{II}-Py was pyrolyzed into Co-N_4 (3.3 wt%), which is purported to be the ORR active site. Electrochemical measurements suggested that Co^{II}/Co^{III} is the redox couple, which is responsible for the catalytic ORR activity. The presence of S is also a beneficial factor for ORR activity.

Regarding the effect of Co content, several catalysts containing different amounts of Co such as $Co_{2\,wt\%}$-$Py_{38\,wt\%}$/C, $Co_{5\,wt\%}$-$Py_{35\,wt\%}$/C, $Co_{10\,wt\%}$-$Py_{30\,wt\%}$/C, $Co_{15\,wt\%}$-$Py_{25\,wt\%}$/C and $Co_{20\,wt\%}$-$Py_{20\,wt\%}$/C, were also synthesized. The optimal Co content in terms of catalytic ORR activity was found to be in the range of 10–15 wt%. As a result from electrochemical measurement using RDE thin film technique and Koutechy–Levich theory, the overall electron transfer number on these catalysts were found to be 3.8–4.0, suggesting the catalyzed ORR is a four-electron transfer process from O_2 to H_2O. More importantly, a cost-effective nitrogen-containing chemical, pyridine, was used as the N-rich ligand for precursor complex formation. Considering that neither Pt nor any other nitrogen-containing ligands with complex structures were involved in the O_2 reduction reaction, the degree of enhancement in both ORR activity and stability seen in these results is significant.

Acknowledgements

This work was supported by the National Natural Science Foundation of China (21173039); Specialized Research Fund for the

Doctoral Program of Higher Education, SRFD (20110075110001) of China; Opening Foundation of Zhejing Provincial Top Key Discipline, China (20110927) and State Environmental Protection Engineering Center for Pollution Treatment and Control in Textile Industry of China, as well as the National Research Council of Canada. All financial support is gratefully acknowledged.

References

[1] W.B. Kim, T. Voitl, G.J. Rodriguez-Rivera, J.A. Dumesic, Science 305 (2004) 1280.
[2] J.L. Fernandez, D.A. Walsh, A.J. Bard, J. Am. Chem. Soc. 127 (2005) 358.
[3] H.R. Colón-Mercado, B.N. Popov, J. Power Sources 155 (2006) 253.
[4] C.W.B. Bezerra, L. Zhang, K. Lee, H. Liu, A.L.B. Marques, E.P. Marques, H. Wang, J. Zhang, Electrochim. Acta 53 (2008) 4937.
[5] Z. Chen, D. Higgins, A. Yu, L. Zhang, J. Zhang, Energy Environ. Sci. 4 (2011) 3167.
[6] M. Lefèvre, E. Proietti, F. Jaouen, J.-P. Dodelet, Science 324 (2009) 71.
[7] G. Wu, K.L. More, C.M. Johnston, P. Zelenay, Science 322 (2011) 443.
[8] R. Bashyam, P. Zelenay, Nature 443 (2006) 63.
[9] E. Proietti, F. Jaouen, M. Lefèvre, N. Larouche, J. Tian, J. Herranz, J.-P. Dodelet, Nature Commun. 2 (2011) 416.
[10] A. Velázquez-Palenzuela, L. Zhang, L. Wang, P.L. Cabot, E. Brillas, K. Tsay, J. Zhang, Electrochim. Acta 56 (2011) 4744.
[11] A. Velazquez-Palenzuela, L. Zhang, L. Wang, P.L. Cabot, E. Brillas, K. Tsay, J. Zhang, J. Phys. Chem. C 115 (2011) 12929.
[12] G. Faubert, G. Lalande, R. Cote, D. Guay, J.-P. Dodelet, L.T. Weng, P. Bertrand, G. Denes, Electrochim. Acta 42 (1996) 1689.
[13] T. Okada, M. Gokita, M. Yuasa, I. Sekine, J. Electrochem. Soc. 145 (1998) 815.
[14] V. Nallathambi, J.W. Lee, S.P. Kumaraguru, G. Wu, B.N. Popov, J. Power Sources 183 (2008) 34.
[15] G. Liu, X.G. Li, P. Ganesan, B.N. Popov, Electrochim. Acta 55 (2010) 2853.
[16] G. Liu, X.G. Li, P. Ganesan, B.N. Popov, Appl. Catal. B: Environ. 93 (2009) 156.
[17] S. Li, L. Zhang, H. Liu, M. Pan, L. Zan, J. Zhang, Electrochim. Acta 55 (2010) 4403.
[18] Z. Shi, H. Liu, K. Lee, E. Dy, J. Chlistunoff, M. Blair, P. Zelenay, J. Zhang, Z.-S. Liu, J. Phys. Chem. C 115 (2011) 16672.
[19] X.G. Li, G. Liu, B.N. Popov, J. Power Sources 195 (2010) 6373.
[20] X.G. Li, B.N. Popov, T. Kawahara, H. Yanagi, J. Power Sources 196 (2011) 1717.
[21] Y. Lu, R.G. Reddy, Electrochim. Acta 52 (2007) 2562.
[22] X. Zhang, K. Tsang, K. Chan, J. Electroanal. Chem. 573 (2004) 1.
[23] N.P. Subramanian, S.P. Kumaraguru, H. Colon-Mercado, H. Kim, B.N. Popov, T. Black, D.A. Chen, J. Power Sources 157 (2006) 56.
[24] H. Niwa, K. Horiba, Y. Harada, M. Oshima, T. Ikeda, K. Terakura, J.I. Ozaki, S. Miyata, J. Power Sources 187 (2009) 93.
[25] Y. Nabae, S. Moriya, K. Matsubayashi, S.M. Lyth, M. Malon, L. Wu, N.M. Islam, Y. Koshigoe, S. Kuroki, M. Kakimoto, S. Miyata, J. Ozaki, Carbon 48 (2010) 2613.
[26] L. Zhu, D. Susac, M. Teo, K.C. Wong, P.C. Wong, P.R. Parsons, D.K. Bizzotto, A.R. Mitchell, S.A. Campbell, J. Catal. 258 (2008) 235.
[27] S. Damyanova, L. Petrov, P. Grange, Appl. Catal. A: General 239 (2003) 241.
[28] U.I. Kramm, I. Herrmann, S. Fiechter, G. Zehl, I. Zizak, I. Abs-Wurmbachc, J. Radnik, I. Dorbandt, P. Bogdanoff, ECS. Trans. 25 (2009) 659.
[29] I. Herrmann, U.I. Kramm, J. Radnik, P. Bogdanoff, S. Fiechter, J. Electrochem. Soc. 156 (2009) B1283.
[30] H.J. Grabke, D. Moszynski, E.M. Müller-Lorenz, A. Schneider, Sur. & Int. Anal. 34 (2002) 369.
[31] S.A. Mamurua, K.I. Ozoemena, T. Fukuda, N. Kobayashi, T. Nyokong, Electrochim. Acta 55 (2010) 6367.
[32] S.Y. Wang, D.S. Yu, L.M. Dai, J. Am. Chem. Soc. 133 (2011) 5182.
[33] R.E. Davis, G.L. Horvath, C.W. Tobias, Electrochim. Acta 12 (1967) 287.